Fano Resonance by Symmetry Breaking Stub in a Metal-Dielectric-Metal Waveguide

2014 Chinese Phys. Lett. 31 057301

(http://iopscience.iop.org/0256-307X/31/5/057301)

CHIN. PHYS. LETT. Vol. 31, No. 5 (2014) 057301

Fano Resonance by Symmetry Breaking Stub in a Metal-Dielectric-Metal Waveguide *

TANG Dong-Hua(汤冬华)[1]**, DING Wei-Qiang(丁卫强)[2]

[1]*Department of Physics, Northeast Forestry University, Harbin 150040*
[2]*Department of Physics, Harbin Institute of Technology, Harbin 150001*

(Received 13 January 2014)

The coupling of a stub obliquely intersected with a metal-dielectric-metal plasmonic waveguide is investigated by using the finite difference in time domain method. Results show that an odd mode, except for the usual even mode, is excited in the stub due to the symmetry breaking of the oblique intersection. Moreover, the results show that the quality factor of the odd mode is very high in comparison with that of the usual even mode, which is then explained by the symmetry breaking of the oblique stub intersection. The superposition of the even and the odd mode generates a Fano shaped spectrum with a very narrow linewidth. The effect of metallic loss and compensation are also discussed. Both the stub and the waveguide are compact in size, and simple in structure, which are beneficial for the achievements of narrow band filtering, sensing, lasing, and nonlinearity enhancement.

PACS: 73.20.Mf, 42.82.Et, 42.79.Ci DOI: 10.1088/0256-307X/31/5/057301

Recently, sub-wavelength plasmonic waveguides formed by metal-dielectric-metal (MDM) layers have been investigated intensively due to their ability of guiding and confining light into a deep sub-wavelength scale through the excitation of surface plasmon polaritons (SPPs).[1,2] In addition to the localization and guiding of photons, many more complex functionalities have been proposed also when extra fine structures are introduced, such as channel drop filtering,[3−8] slow light propagation,[9,10] electro-optical modulation,[11,12] sensing,[13] and bistable switching.[14] Among those functional devices, plasmonic stubs[15−24] may be the simplest while the most powerful construction element, which is just a segment of MDM waveguide branch that partially reflects the SPPs transmitting through it. The waveguide-stub structures are also widely used in compact optical filtering and trapping.[19−24]

Generally speaking, all the stubs that have been proposed are perpendicular with the main MDM plasmonic waveguide (i.e., $\theta = 90°$ in Fig. 1), and most of them lie on one side of the waveguide only. In this case, the stubs just behave like broadband reflectors, which result in very wide (more than several hundreds of nanometers) dips in the transmission spectra. This weak interaction is not suitable for compact filtering, sensing, lasing, and high quality factor (Q) cavities. To achieve a stronger interaction and high Q cavities, multiple stubs should be introduced to form Bragg grating like reflections.[16,17] This, however, makes the structure rather complex.

In this Letter, we show that two short stubs (in other words, one stub intersects with the main plasmonic channel) are enough to form high Q SPP cavities and narrow band filtering, provided that the two stubs lie to the two sides of and are oblique with respect to the main MDM waveguide, as shown in Fig. 1. Our results show that Fano resonance with a line width of less than 1 nm (in the case of lossless material, or the loss is compensated for by gains) may be achieved when the stubs are introduced at a specified oblique angle θ. For the perpendicular stubs, the Fano resonance can be obtained only when higher modes are excited simultaneously, and the multi-mode interference occurs in the stubs, which requires the size of the stubs to be rather large.[23,25] We find the physical origins from the symmetry breaking of the oblique structure, which agree well with the numerical results of finite difference in the time domain (FDTD) method.[26] This structure provides a promising candidate for the filtering, sensing, lasing, and nonlinearity enhancement in deep sub-wavelength plasmonic structures.

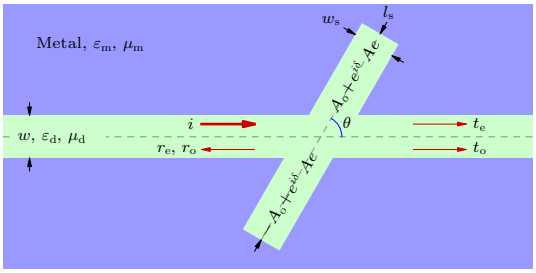

Fig. 1. (Color online) Schematic structure of an oblique stub intersected with a metal-dielectric-metal (MDM) plasmonic waveguide. The relative permittivity and relative permeability of the dielectric (metal) are ε_d (ε_m) and μ_d (μ_m), respectively. The stub with dimensions of w_s and l_s intersects with the main plasmonic waveguide (with a width of w) at an oblique angle of θ. The red arrows of i, $r_{e,o}$ and $t_{e,o}$ show the incident, reflections and transmissions, and the subscribes o and e represent the odd and even modes of the stub, respectively.

Figure 1 shows the schematic structure investigated in this work. The MDM plasmonic waveguide is

*Supported by the Fundamental Research Funds for the Central Universities under Grant No DL11BB23.
**Corresponding author. Email: dhtanghit@126.com

formed by a dielectric layer sandwiched by two infinite metallic layers. The stub is introduced with an angle θ with respect to the axis of the MDM waveguide ($+x$-axis). Different from the waveguide-stub structures that have already been investigated, the crossing angle θ is not 90° in our case. The size of the waveguide and the stub are w, w_s and l_s, respectively, as marked in Fig. 1. Without loss of generality, suppose that the plasmonic waveguide and the stubs are filled with air ($\varepsilon_d = 1.0$ and $\mu_d = 1.0$). The metal layers are silver described by the Drude model (Palik data)[27] with a relative permeability $\mu_m = 1.0$ and permittivity $\varepsilon_m = \varepsilon_\infty + \omega_p^2/[\omega(\omega + i\gamma_p)]$, respectively. Using the FDTD,[26] we simulate the transmission spectra of the structure with different parameters, and the results are shown in Fig. 2.

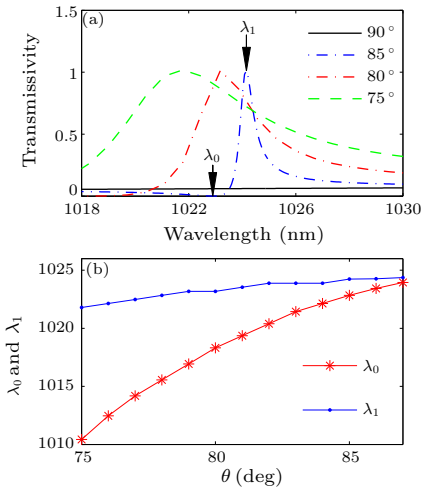

Fig. 2. (Color online) (a) Transmission spectra of the plasmonic stub-waveguide coupling structure at different oblique angles of $\theta = 90°$ (black, solid curve), 85° (blue, dash-dotted), 80° (red, dash-dotted), and 75° (green, dashed). (b) Change of wavelength $\lambda_{0,1}$ ($T(\lambda_0) = 0$ and $T(\lambda_1) = 1$, as marked in (a)) with the oblique angle θ.

The parameters used in the simulation results of Fig. 2 are $w = w_s = 50\,\text{nm}$, $l_s = 350\,\text{nm}$, $\omega_p = 2.7 \times 10^{16}\,\text{Hz}$, and θ changes from 75° to 90°. The loss of silver is ignored temporarily, and its effect will be discussed separately in the following. Figure 2(a) shows the transmission spectrum of the structure with different oblique angles of $\theta = 75°$ (green and dashed curve), 80° (red and dash dotted), 85° (blue and dash-dotted), and 90° (black and solid). At the usual case of $\theta = 90°$, there is a very wide dip in the transmission spectrum T (about 800 nm–1300 nm, not shown the whole spectrum range in Fig. 2(a) for clarity), which results from the broadband reflection of the stubs.[15–17] When the stubs are oblique with an angle of $\theta = 75°$, as shown by the green dashed line in Fig. 2(a), an asymmetric Fano-like resonance appears in the background of the wide and slow dip mentioned above. With the increase of θ from 75° to 85°, the line width $\delta\lambda$ (the full width at half maxima (FWHM)) of the resonant mode decreases rapidly from 5 nm to less than 1 nm. Figure 2(b) shows the changes of λ_0 and λ_1 with the oblique angle θ. Here $\lambda_{0,1}$ are the two wavelengths, at which the transmission coefficients are minimum and maximum, respectively. One can see that $\lambda_1 - \lambda_0$ tends to be zero rapidly with the increase of θ from 75° to 90°.

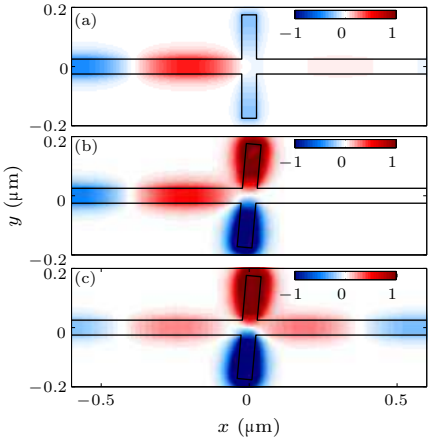

Fig. 3. (Color online) Field patterns of $H_z(x, y)$ at different cases. (a) $H_z(x, y)$ for the case of $\theta = 90°$ at the wavelength of λ_0 marked in Fig. 2(a). (b) The same as (a) but for $\theta = 85°$. (c) The same as (a) but at the wavelength of λ_1. Other parameters are $w = w_s = 50\,\text{nm}$, $l_s = 350\,\text{nm}$, $\varepsilon_d = 1$, and $\mu_d = 1$. The metal is silver with ε_m formulated by the Drude model (see text for details).

To show the transmission of light in the structure more clearly, we plot the magnetic field pattern of $H_z(x, y)$ for the two special wavelengths of λ_0 and λ_1, as shown in Figs. 3(a), 3(b) and 3(c), respectively. Figure 3(a) shows the field pattern of $\theta = 90°$ at the wavelength of λ_0. One can see that the transmission is very low, which results from the reflection of the oblique stub. One can also find that the field localizations in the two stubs are in phase, and do not enhance obviously in comparison with the incident field. In the case of $\theta = 85°$, however, the field localizations in the two stubs are enhanced greatly by a factor of 20, and also the two stubs are out of phase (shown by red and blue colors, respectively), as shown in Fig. 3(b). At the wavelength of λ_1, similar situations are observed, except for the transmission coefficient, which approaches 1, as shown in Fig. 3(c). The quality factor Q in this case is about $\lambda_0/\delta\lambda \sim 1500$, which is much larger than the case of ring and disk resonators in the plasmonic platform.[3–8] More importantly, one can also find that the resonant spectrum is an asymmetric Fano shape,[28] while not a symmetric Lorentzian shape. This sharp asymmetric resonance may be very useful in the design of filtering and sensing.[29,30]

We contribute the narrow band Fano resonance to the coupling between the two oblique and face-to-face stubs. At the usual case of $\theta = 90°$, the structure is symmetric about the axis, and the mode inside the stubs is also even when the MDM waveguide is excited by a symmetric source. When $\theta \neq 90°$, however, the mirror symmetry about the axis is broken, and the odd mode may also be excited except for the usual even mode. For the even mode, the Q factor is

very low due to the broadband reflection feature of the stubs. For the odd mode, however, the Q factor can be very high due to the interference confinement of the mode.[29,30] We know that the Q factor is determined by the dissipation rate of the light energy stored in the stubs. In the case of the odd mode, the fields in the two stubs are out of phase, and then the dissipations of them interfere destructively in the output channel.[31,32] Therefore, a very low dissipation rate is obtained for the odd mode, which results in the high Q factor.

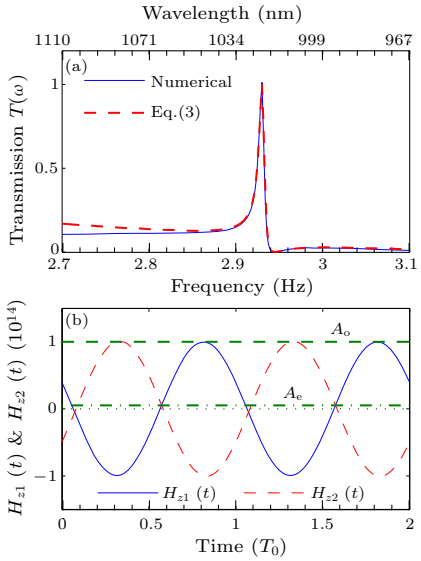

Fig. 4. (Color online) (a) Comparison of numerical result (blue and solid line) with that of Eq. (3) (red and dashed) in the case of $\theta = 80°$. The resonant centers, line widths, and the excitation ratio of the even and odd modes used in Eq. (3) are $\omega_{0e} = 330.0$ THz and $\omega_{0o} = 293.1$ THz, $\gamma_e = 110$ THz, $\gamma_o = 0.367$ THz, and $c_e/c_o = 0.82$, respectively. See text for the details of those parameters. (b) Temporal evolutions of the magnetic field in the two stubs, and the amplitudes of the even (A_e) and odd (A_o) modes calculated by using Eq. (4).

The even mode with a very low Q factor provides a continuous spectrum background, while the high Q odd mode provides a discrete mode. It is know that the interference of a discrete mode and a continuous mode can generate a Fano shaped spectrum.[28–30] For the case of the even mode, the structure can be regarded as a waveguide side-coupled with a low quality cavity. For the odd mode, however, the two stubs couple strongly, and behave like a single inline coupled cavity. Using the coupled mode theory (CMT), one can obtain the transmission spectra of t_e and t_o for these two modes,[33,34]

$$t_e = \frac{\omega - \omega_{0e}}{\omega - \omega_{0e} + i\gamma_e}, t_o = \frac{i\gamma_o}{\omega - \omega_{0o} + i\gamma_o}, \quad (1)$$

where $\omega_{0e,0o}$ and $\gamma_{e,o}$ are the resonant frequency centers, and dissipation factors of the even and odd modes, respectively. Finally, the total transmission spectrum should be the superposition of the two modes, which is

$$\begin{aligned} T &= |t|^2 = |c_e t_e + c_o t_o|^2 \\ &= \left| \frac{c_e(\omega - \omega_{0e})}{\omega - \omega_{0e} + i\gamma_e} + \frac{ic_o\gamma_o}{\omega - \omega_{0o} + i\gamma_o} \right|^2, \end{aligned} \quad (2)$$

where the coefficients $c_{o,e}$ reveal the excitation probabilities of the odd and even modes when the source is launched from the left port. Due to the two modes being excited by the same excitation source and in the same structure, c_o and c_e should be real numbers, and satisfy the relation of $c_o^2 + c_e^2 = 1$ for the reason of energy conservation. According to the properties of the two modes analyzed above (and also shown in the numerical simulation results), we have the relationship of $\gamma_e \gg \gamma_o$. Because γ_o is very small, $\omega - \omega_{0e}$ may be replaced by $\omega_{0o} - \omega_{0e}$ near the resonant center of ω_{0o} at the first order of approximation. Therefore, Eq. (2) can be reduced to the following form of

$$\begin{aligned} T &= \left| \frac{c_e(\omega - \omega_{0e})}{\omega - \omega_{0e} + i\gamma_e} + \frac{ic_o\gamma_o}{\omega - \omega_{0o} + i\gamma_o} \right|^2 \\ &= |[c_e(\omega - \omega_{0e})(\omega - \omega_{0o}) + i\gamma_o(c_e + c_o)(\omega - \omega_{0e}) \\ &\quad - c_o\gamma_o\gamma_e]/[(\omega - \omega_{0e} + i\gamma_e)(\omega - \omega_{0o} + i\gamma_o)]|^2 \\ &\approx [|c_e(\omega_{0o} - \omega_{0e})|^2]/[(\omega_{0o} - \omega_{0e})^2 + \gamma_e^2] \\ &\quad \cdot \left\{ \left[\omega - \omega_{0o} - \frac{c_o\gamma_o\gamma_e}{c_e(\omega_{0o} - \omega_{0e})} \right]^2 \right. \\ &\quad \left. + \gamma_o^2 \left(1 + \frac{c_o}{c_e} \right)^2 \right\} / [(\omega - \omega_{0o})^2 + \gamma_o^2] \\ &= T_0 \frac{(\omega - \omega_0 + f\gamma_o)^2}{(\omega - \omega_0)^2 + \gamma_o^2} + T_b, \end{aligned} \quad (3)$$

which shows that the transmission spectrum is formed by a standard Fano resonance term and a background of T_b. For the standard Fano term, the linewidth is the same as that of the odd mode γ_o, and the Fano factor is $f = c_o\gamma_e/[c_e(\omega_{0e} - \omega_{0o})]$, which is related to the frequency separation between the resonant centers of the two modes, and also the excitation ratio of the two modes. We check the background term T_b numerically, and find that it is a very small value in our cases, which does not change the Fano shape of the spectrum.

We compare Eq. (3) with the numerical results, and the results are shown in Fig. 4. In Fig. 4(a), the blue curve shows the numerical spectrum at $\theta = 80°$ (the same as the red line in Fig. 2(a)). From the numerical spectrum of the even mode and the Fano mode, we can read directly the resonant centers of them, which are $\omega_{0e} = 330.0$ THz and $\omega_{0o} = 293.1$ THz, respectively. What is more, using the curve fitting method, we can also extract the dissipation factors of $\gamma_e = 110$ THz, $\gamma_o = 0.367$ THz approximately from the numerical results and Eq. (1). Then we use the standard Fano resonant spectrum to fit the numerical result of Fig. 4(a), and an optimized Fano factor of $f = 3.8$ is obtained, which means the excitation ratio of $c_e/c_0 = 0.8$, according to the relation of $f = c_o\gamma_e/[c_e(\omega_{0e} - \omega_{0o})]$. One can find that

they agree quite well with each other near the resonant center. This result shows that the mode superposition interpretation is suitable for this structure.

According to this mechanism, the field amplitudes in the two stubs should be $A_o + e^{i\delta}A_e$ and $-A_o + e^{i\delta}A_e$ (as marked in Fig. 1), respectively, which means that the field intensities in the two stubs are not equal. Here $A_{o,e}$ and δ represent the amplitude of the odd and even modes in the stubs, and the phase difference between them, respectively. This inequality can be verified easily by checking the field profiles in the two stubs shown in Figs. 3(b) and 3(c). According to the above analysis, the temporal evolutions of the magnetic field in the two stubs are $H_{z1}(t) = (A_o + e^{i\delta}A_e)e^{-i\omega t}$ and $H_{z2}(t) = (-A_o + e^{-i\delta}A_e)e^{-i\omega t}$, respectively. Here ω is the angular frequency of the signal. Then we obtain the amplitudes of the two modes,

$$A_o = \frac{1}{2}[H_{z1}(t) - H_{z2}(t)]e^{i\omega t},$$
$$e^{i\delta}A_e = \frac{1}{2}[H_{z1}(t) + H_{z2}(t)]e^{i\omega t}. \quad (4)$$

By using the numerical method, $H_{z1,2}(t)$ can be obtained easily. Then we can calculate A_o and A_e using Eq. (4). For example, for the state shown in Fig. 3(c), we calculate $H_{z1,2}(t)$ numerically, as shown in Fig. 4(b). Using Eq. (4), the results of $A_o = 1$ (normalized), $A_e = 0.053$ and $\delta = 95°$ are obtained. Considering the fact of $\gamma_e/\gamma_o \sim 300$ and $|A_e/A_o|^2 \sim 1/356$, the excitation ratio of the two modes should be about 0.84, which agrees well with $c_{e,o}$ used above.

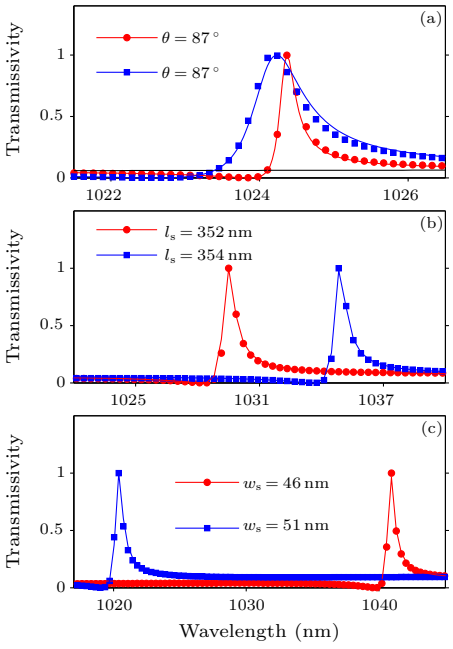

Fig. 5. (Color online) Tuning and Fano curve fitting of the transmission spectra: (a) transmissions for $\theta = 87°$ and $85°$ with $l_s = 350$ nm and $w_s = 50$ nm fixed, (b) $l_s = 352$ nm and 354 nm with $\theta = 85°$ and $w_s = 50$ nm fixed, (c) $w_s = 46$ nm and 51 nm with $l_s = 350$ nm and $\theta = 85°$ fixed.

The Fano spectrum can be tuned easily by the oblique angle θ as well as the size of the stub w_s and l_s, as shown in Fig. 5. For comparison, we also plot the fitted curve (solid lines) using the standard Fano formula of $T = (\varepsilon + f)^2/(\varepsilon^2 + 1)$,[26–28] where f is the asymmetrical Fano factor, and $\varepsilon = 2(\lambda_0 - \lambda)/\Gamma$ is the wavelength relative to the resonant center λ_0 (scaled by the linewidth Γ). In Fig. 5(a), Fano factors $f = 3.8$ are obtained for both $\theta = 87°$ and $85°$, and linewidths of $\Gamma = 0.2$ nm and 0.65 nm are found for $\theta = 87°$ and $85°$, respectively. This shows that the oblique angle determines the linewidth sensitivity. When the length l_s (w_s) changes (with the oblique angle $\theta = 85°$ fixed), the resonant center λ_0 changes sensitively, as shown in Figs. 5(b) and 5(c). The Fano factor f and the linewidth Γ, however, change very slightly. These properties make tuning the Fano resonance spectrum very easy.

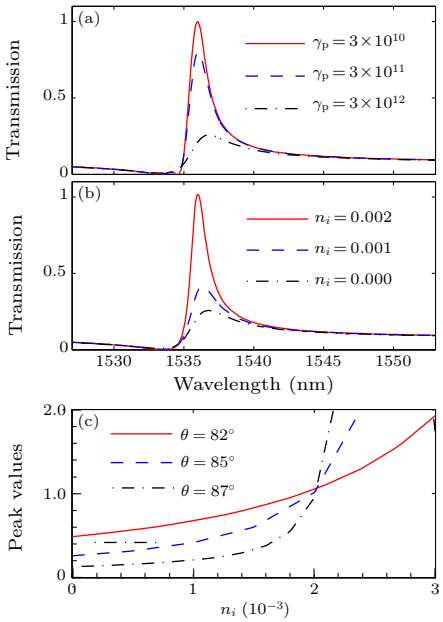

Fig. 6. (Color online) Effects of metallic loss and compensation. The slot and stub regions are filled by a dielectric material with a refractive index of $n = 3.4 + in_i$. The parameters are $w_s = w = 50$ nm, and $l_s = 140$ nm. (a) Transmission spectra at $\theta = 85°$ with different damping factors γ_p. (b) Transmission spectra at $\theta = 85°$ with different gain factors of n_i, while the damping factor $\gamma_p = 3 \times 10^{12}$ Hz is fixed. (c) Transmission peaks with the increase of n_i for different oblique angles.

When the loss of the metal is considered, the transmission spectrum will be modified obviously, as shown in Fig. 6(a). In the simulation of Fig. 6, $w_s = w = 50$ nm, and $l_s = 140$ nm, the slot and the stub regions are filled by a dielectric medium with a refractive index of $n = 3.4$ rather than air (to introduce material gains). With the increase of γ_p (the dissipation factor in the Drude model), both the transmission coefficients and the Q factors decrease rapidly and the resonant peak may vanish when γ_p is large enough. The metallic loss can be compensated for by two different methods. First, one can decrease the oblique

angle θ to weaken the resonance of light in the stubs (with a price of decreasing the Q factor). Second, the metallic loss can be compensated for by introducing gains to the dielectric material filled in the slot and the stubs, as shown in Figs. 6(b) and 6(c). We use an imagery part n_i (i.e., $n = 3.4 + in_i$) to tune the gain, and the metal loss is fixed at $\gamma_{\rm p} = 3 \times 10^{12}$ Hz. Figure 6(b) shows the transmission spectrum at $\theta = 85^\circ$ with different n_i, and in the case of $n_i = 0.002$, the metal loss is completely compensated for by the gain. Figure 6(c) shows the changes of transmission peak value with n_i for different oblique angles θ. When n_i >0.002, net gains are obtained, which may be used as lasing and active sensing on the nano scale.

In summary, we have proposed a simple while efficient method to excite high quality factor modes in the stub-waveguide plasmonic structure by introducing a pair of oblique stubs to the MDM plasmonic waveguide. High Q factor for the odd mode is obtained due to the destructive cancelling of the dissipation of the odd mode. The superposition of the odd and even modes generates an asymmetric Fano spectrum, which is described by a mode coupling formula. When the metallic loss is considered, the high quality factor and Fano shaped modes can still be obtained with moderate gain compensation. By using this high Q cavity, many applications such as narrow band filtering, highly sensitive sensing, lasing, and nonlinearity enhancement can be achieved in a deep sub-wavelength scale.

References

[1] Bozhevolnyi S I, Volkov V S, Devaux E, Laluet J Y and Ebbesen T W 2006 *Nature* **440** 508
[2] Gramotnev D K and Bozhevolnyi S I 2010 *Nat. Photon.* **4** 83
[3] Xiao S, Liu L and Qiu M 2006 *Opt. Express* **14** 2932
[4] Hosseini A and Massoud Y 2007 *Appl. Phys. Lett.* **90** 181102
[5] Wang T, Wen X, Yin C and Wang H 2009 *Opt. Express* **17** 24096
[6] Han Z, Van V, Herman W N and Ho P T 2009 *Opt. Express* **17** 12678
[7] Holmgaard T, Chen Z, Bozhevolnyi S I, Markey L and Dereux A 2009 *Opt. Express* **17** 2968
[8] Volkov V S, Bozhevolnyi S I, Devaux E, Laluet J Y and Ebbesen T W 2007 *Nano Lett.* **7** 880
[9] Yang L, Min C and Veronis G 2010 *Opt. Lett.* **35** 4184
[10] Huang Y, Min C and Veronis G 2011 *Appl. Phys. Lett.* **99** 143117
[11] Thomas R, Ikonic Z and Kelsall R W 2011 *Photon. Nanostruct. Fundam. Appl.* **9** 101
[12] Zhu Y J, Huang X G and Mei X 2012 *Chin. Phys. Lett.* **29** 064214
[13] Zhu J H, Huang X G and Mei X 2011 *Chin. Phys. Lett.* **28** 054205
[14] Pannipitiya A, Rukhlenko I D and Premaratne M 2011 *J. Opt. Soc. Am.* B **28** 2820
[15] Pannipitiya A, Rukhlenko I D and Premaratne M 2011 *IEEE Photon. J.* **3** 220
[16] Pannipitiya A, Rukhlenko I D, Premaratne M, Hattori H T and Agrawal G P 2010 *Opt. Express* **18** 6191
[17] Liu J, Fang G, Zhao H, Zhang Y and Liu S 2009 *Opt. Express* **17** 20134
[18] Piao X, Yu S, Koo S, Lee K and Park N 2011 *Opt. Express* **19** 10907
[19] Mirnaziry S R, Setayesh A and Abrishamian M S 2011 *J. Opt. Soc. Am.* B **28** 1300
[20] Lu H, Liu X, Gong Y, Mao D and Wang G 2011 *J. Opt. Soc. Am.* B **28** 1616
[21] Chen J, Li Z, Li J and Gong Q 2011 *Opt. Express* **19** 9976
[22] Chen P, Liang R, Huang Q and Xu Y 2011 *Opt. Commun.* **284** 4795
[23] Chen J, Sun C and Gong Q 2014 *Opt. Lett.* **39** 52
[24] Zeng C and Cui Y 2013 *Opt. Commun.* **290** 188
[25] Chen Z Q, Qi J W, Chen J, Li Y D, Hao Z Q, Lu W Q, Xu J J and Sun Q 2013 *Chin. Phys. Lett.* **30** 057301
[26] Taflove A and Hagness S C 2005 *Comput. ElectroDyn.: Finite-Difference Time-Domain Method* 3rd edn (Norwood: Artech House)
[27] Palik E 1985 *Handbook of Optical Constants of Solids* (San Diego: Academic Press)
[28] Fano U 1961 *Phys. Rev.* **124** 1866
[29] Miroshnichenko A E, Flach S and Kivshar Y S 2010 *Rev. Mod. Phys.* **82** 2257
[30] Luk'yanchuk B, Zheludev N I, Maier S A, Halas N J, Nordlander P, Giessen H and Chong C T 2010 *Nat. Mater.* **9** 707
[31] Feigenbaum E and Atwater H A 2010 *Phys. Rev. Lett.* **104** 147402
[32] Endo S, Oka T and Aoki H 2010 *Phys. Rev.* B **81** 113104
[33] Xu Y, Li Y, Lee R K and Yariv A 2000 *Phys. Rev.* E **62** 7389
[34] Fan S, Villeneuve P R, Joannopoulos J D, Khan M J, Manolatou C and Haus H A 1999 *Phys. Rev.* B **59** 15882